Phasonic Spectroscopy of a Quantum Gas in a Quasicrystalline Lattice

Shankari V. Rajagopal, Toshihiko Shimasaki, Peter Dotti, Mantas Račiūnas, Ruwan Senaratne, Egidijus Anisimovas, André Eckardt, and David M. Weld

Phys. Rev. Lett. **123**, 223201 — Published 25 November 2019

DOI: 10.1103/PhysRevLett.123.223201

Phasonic Spectroscopy of a Quantum Gas in a Quasicrystalline Lattice

Shankari V. Rajagopal,[1] Toshihiko Shimasaki,[1] Peter Dotti,[1] Mantas Račiūnas,[2] Ruwan Senaratne,[1] Egidijus Anisimovas,[2] André Eckardt,[3] and David M. Weld[1,*]

[1] *Department of Physics, University of California, Santa Barbara, California 93106, USA*
[2] *Institute of Theoretical Physics and Astronomy, Vilnius University, Saulėtekio 3, LT-10257 Vilnius, Lithuania*
[3] *Max-Planck-Institut für Physik komplexer Systeme, Nöthnitzer Str. 38, 01187 Dresden, Germany*

Phasonic degrees of freedom are unique to quasiperiodic structures, and play a central role in poorly-understood properties of quasicrystals from excitation spectra to wavefunction statistics to electronic transport. However, phasons are challenging to access dynamically in the solid state due to their complex long-range character and the effects of disorder and strain. We report phasonic spectroscopy of a quantum gas in a one-dimensional quasicrystalline optical lattice. We observe that strong phasonic driving produces a nonperturbative high-harmonic plateau strikingly different from the effects of standard dipolar driving. Tuning the potential from crystalline to quasicrystalline, we identify spectroscopic signatures of quasiperiodicity and interactions and map the emergence of a multifractal energy spectrum, opening a path to direct imaging of the Hofstadter butterfly.

Phasons are degrees of freedom unique to quasicrystals [1–5]. The role of phasons in determining quasicrystal properties remains incompletely understood: open questions include the effects of electron-phason coupling, the nature of electronic transport, spectral statistics, topological properties, and even the shape of the electronic wavefunctions [6–15]. These lacunae are in part due to the theoretical intractability of quasiperiodic matter, and in part due to the experimental difficulty of disentangling the effects of domain walls, crystalline impurities, and disorder from those due to phason modes, which arise from broken translation symmetry in the in the higher-dimensional space from which the quasiperiodic lattice is projected. The exquisite controllability of ultracold atoms in optical lattices makes them well-suited to the study of quasicrystal phenomena from structure to transport to self-similarity [16–25]. Beyond the fundamental interest of such questions, they may point the way to technological applications of quasicrystals' anomalous electrical and thermal transport characteristics.

Here we report the realization of phasonic spectroscopy on a one-dimensional quasicrystal, using a quantum gas in a tunable bichromatic optical lattice. In addition to standard dipolar modulation, the experiment enables dynamic driving of a phasonic degree of freedom [26, 27] via modulation of the relative spatial phase between the two sublattices. We observe that the quasicrystal responds very differently to dipolar and phasonic drives: most strikingly, phasonic modulation generates a broad non-perturbative plateau of high-order "multi-photon" transitions, in which multiple energy quanta ("photons") with energy corresponding to the driving frequency are absorbed. To further elucidate the spectroscopic signatures of quasicrystallinity we measure excitation spectra while varying the strength of quasiperiodicity through a localization transition, observing the emergence of minibands, identifying spectral features arising from interatomic interactions and localization-induced diabaticity, and mapping a slice of the Hofstadter butterfly energy spectrum.

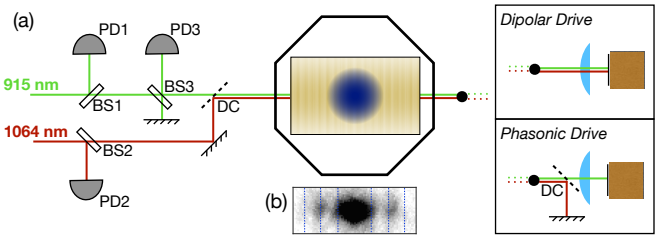

FIG. 1. Experimental schematic. (a)BEC (blue) in a bichromatic lattice (yellow). Photodiodes (PD), beam samplers (BS), and dichroic mirrors (DC) are indicated, as is the configuration for both dipolar and phasonic driving using a piezo-driven mirror (solid block). (b) Sample band-mapped data. Dotted lines indicate zone edges of the primary lattice.

The experiments (diagrammed in Fig. 1) use a 1D bichromatic potential which superposes a primary and secondary lattice formed by light with wavelengths $\lambda_P = 1064$ nm and $\lambda_S = 915$ nm. Neglecting interactions, the Hamiltonian of atoms in this potential is

$$H = -\frac{\hbar^2}{2m}\frac{d^2}{dx^2} + \frac{V_P}{2}\cos(2k_P(x-\delta_P)) + \frac{V_S}{2}\cos(2k_S(x-\delta_S)), \quad (1)$$

where $k_{P(S)} = 2\pi/\lambda_{P(S)}$ and V_P and δ_P (V_S and δ_S) are the amplitude and spatial phase of the primary (secondary) lattice. For $V_P \gg V_S$, in the tight-binding limit with respect to the primary lattice, this Hamiltonian is closely related to both the Aubry-André model [28] and the Harper model [29]; for larger V_S, deviations from these models appear in the form of mobility edges [30–33]. Lattice depths are measured in the respective recoil

* weld@ucsb.edu

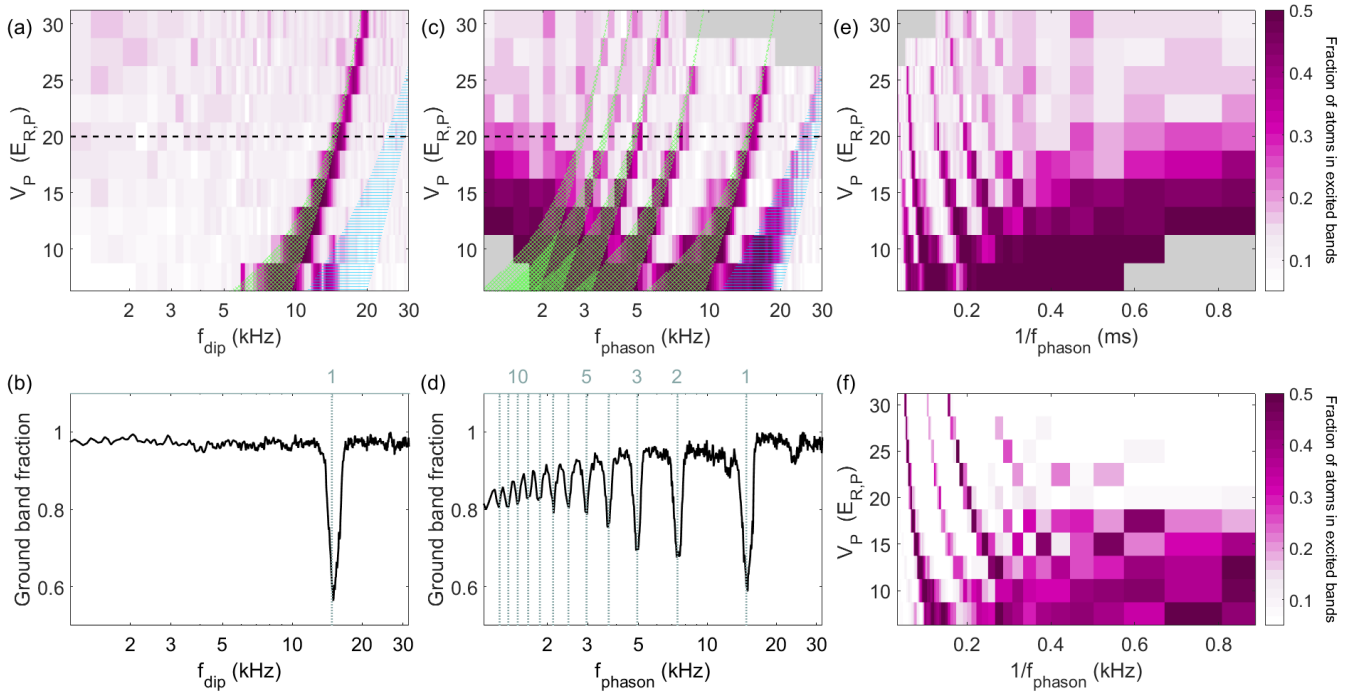

FIG. 2. Comparison of dipolar and phasonic spectroscopy; areas where no data was taken are marked in gray. **(a)** Excitation due to dipolar driving as a function of drive frequency $f_{\rm dip}$ and primary lattice depth V_P with $\alpha_{\rm dip} = 0.16 \times V_S/V_P$ and $V_S = 1E_{R,S}$. Green hatched (Blue horizontal) overlay shows calculated first (second) interband transition. **(b)** High-resolution dipolar spectrum at $V_P = 20E_{R,P}$. Line shows the calculated center of the first interband transition. **(c)** Excitation due to phasonic driving as a function of drive frequency $f_{\rm phason}$ and primary lattice depth V_P. $\alpha_{\rm phason}$ is set to ≈ 1. Green hatched (Blue horizontal) overlays show calculated first (second) interband transition, with multiphoton subharmonics also indicated for the first transition. **(d)** High-resolution phasonic spectrum at $V_P = 20E_{R,P}$. Lines show the calculated center of the first twelve multiphoton transitions corresponding to the lowest interband transition. **(e)** Data from (c) plotted versus drive period $1/f_{\rm phason}$, showing a broad low-frequency absorption feature. **(f)** Theoretical prediction for (e) (details in text).

energies, $E_{R,i} = \hbar^2 k_i^2/2m$, $i \in \{P, S\}$. The chosen value of the ratio $\nu = \lambda_S/\lambda_P$ is effectively irrational in the sense that it gives rise to a unit cell larger than our 30 μm sample size; in other words, the potential is quasiperiodic to within experimental resolution.

A key feature of the experiment is the ability to modulate the different degrees of freedom of the bichromatic lattice. Standard dipolar excitation, which drives the lowest-energy phononic mode of the lattice, is achieved by equal translation of both lattices:

$$\delta_S(t) \;=\; \delta_P(t) \;=\; A_{\rm dip}\sin(2\pi f_{\rm dip} t), \qquad (2)$$

where $A_{\rm dip}$ and $f_{\rm dip} = \omega_{\rm dip}/2\pi$ are the amplitude and frequency of the dipolar drive. In the lattice frame the force applied to the atoms is $F(t) = F_0 \sin(2\pi f_{\rm dip} t)$ for $F_0 = m(2\pi f_{\rm dip})^2 A_{\rm dip}$. Using the primary lattice constant $a = \lambda_P/2$, we define a dimensionless driving parameter $\alpha_{\rm dip} = aF_0/\hbar\omega_{\rm dip} = am\omega_{\rm dip}A_{\rm dip}/\hbar$ (which determines the modification of tunnelling matrix elements in the lowest band [34]). To keep $\alpha_{\rm dip}$ fixed for different drive frequencies, we take $A_{\rm dip} \propto 1/f_{\rm dip}$; this normalization procedure for phase modulation has been used previously to study multiphoton excitations in a single-color lattice [35, 36]. Phasonic modulation is achieved by translating only the secondary lattice:

$$\delta_S(t) = A_{\rm phason}\sin(2\pi f_{\rm phason} t), \qquad \delta_P(t) = 0, \qquad (3)$$

where $A_{\rm phason}$ and $f_{\rm phason}$ are the amplitude and frequency of the phasonic drive. As with the dipolar drive, we define a dimensionless amplitude $\alpha_{\rm phason}$, for which $A_{\rm phason} = C\alpha_{\rm phason}/f_{\rm phason}$, taking $C = 1000$ nm · kHz.

We report spectroscopic measurements of the quasicrystal's response to phasonic and dipolar excitation with varying drive and lattice parameters. The experiments begin by adiabatically loading a Bose condensate of ^{84}Sr into the bichromatic lattice. The amplitude of dipolar or phasonic modulation is linearly ramped to the final value over 4 ms, followed by constant-amplitude modulation for 16 ms. After modulation, both lattices are ramped down simultaneously at a rate which is adiabatic with respect to the energy gaps of the primary lattice, to achieve approximate band mapping onto free-space momentum states [37]. This enables measurement of the primary spectroscopic observable: the fractional population of atoms in the ground band of the primary lattice after modulation.

As a first application of phasonic spectroscopy, we measure and plot in Fig. 2 the difference between a quasicrystal's response to standard dipolar driving and its response to phasonic driving. We fix the phasonic driving amplitude to $\alpha_{\mathrm{phason}} \approx 1$. To facilitate comparison, the dipolar drive is scaled with respect to the phasonic one by a factor proportional to the sublattice depth ratio: $\alpha_{\mathrm{dip}} = 0.16 \times V_S/V_P$. V_S is held at $1E_{R,S}$ for both drives. Dipolar driving causes excitations to higher bands which are consistent with expected interband transitions of the primary lattice (Fig. 2(a) and 2(b)). The second interband transition is visible but suppressed compared to the first transition, since the odd-parity dipolar force does not couple unperturbed Wannier states of the primary lattice of equal parity on the same site. No multiphoton transitions are apparent at this drive amplitude.

The response to phasonic driving is qualitatively different, although due to the chosen α scaling the main interband transition is driven at similar strength. Most strikingly, we observe strong multiphoton processes up to the twelfth order (Fig. 2(c) and 2(d)). Phasonic excitation in this regime apparently gives rise to an efficient high-harmonic response, in which atoms can absorb energy at high multiples of the drive frequency. Additionally, comparison of Fig. 2(a) and 2(c) indicates that phasonic driving appears to relax the suppression of even interband transitions, which we attribute to the fact that it is not parity (anti)symmetric on site. Finally, we observe a broad low-frequency absorption feature at large tunneling amplitudes in the phasonic spectrum. This feature, most easily seen in Fig. 2(e), is likely due to overlap of numerous high-order harmonics. The experimental results in Fig. 2(e) are reproduced well by the non-interacting exact time-evolution numerical simulations shown in Fig. 2(f) [38]. The experimental observation of these unique features of phasonic spectroscopy of a tunable quantum quasicrystal — efficient high-harmonic response, relaxed selection rules, and broadband IR absorption — constitute the first main result of this report.

The proliferation of multiphoton resonances is connected to the breakdown of the regime where the driving amplitude can be treated perturbatively [39]. In the phasonically excited quasicrystal, the threshold for entering the non-perturbative regime can be estimated by expanding the shaken secondary lattice potential as $\cos(2k_S[x - A\sin(\omega t)]) = \sum_{n=-\infty}^{\infty} J_n(2k_S A)[\cos(2k_S x)\cos(n\omega t) + \sin(2k_S x)\sin(n\omega t)]$, where the Bessel functions J_n contain all powers (orders) of the scaled driving amplitude $2k_S A = (4\pi k_S C/\omega)\alpha_{\mathrm{phason}}$. The individual terms can directly induce n-photon transitions with $\Delta E = |n|\hbar\omega$, but (as a property of the Bessel function) contribute only as long as long as $|n| \lesssim 2k_S A$, corresponding to the estimated threshold value $\alpha_{\mathrm{th}} = \Delta E/4\pi\hbar k_S C$ for the dimensionless driving amplitude α_{phason}. For transitions to the first excited band, we obtain α_{th} close to unity [38], in reasonable agreement with both the numerical simulations shown in Fig 3(a) and the experimental data shown in Fig. 3(b). Note in particular that at low frequencies, in order to keep α_{phason} constant and equivalent to that used for the dipolar drive, the position-space amplitude of the phasonic drive used for the data shown in Fig. 2 increases to significantly more than one lattice constant. A noticeable difference between the dipolar and the phasonic drive is the significantly flatter distribution of transition strengths in the phasonic case. As an experimental indication of this effect, note the comparison of dipolar and phasonic spectra in Fig. 3(c): while the high-amplitude phasonic spectrum shows numerous narrow transition lines, a dipolar spectrum taken at an amplitude sufficient to weakly drive multiphoton transitions already exhibits extreme power-broadening of the first interband transition, in agreement with previous work on periodic lattices [35, 36]. As an additional point of interest, we note that connections between harmonic generation and quasiperiodicity have been made in other physical systems [40, 41].

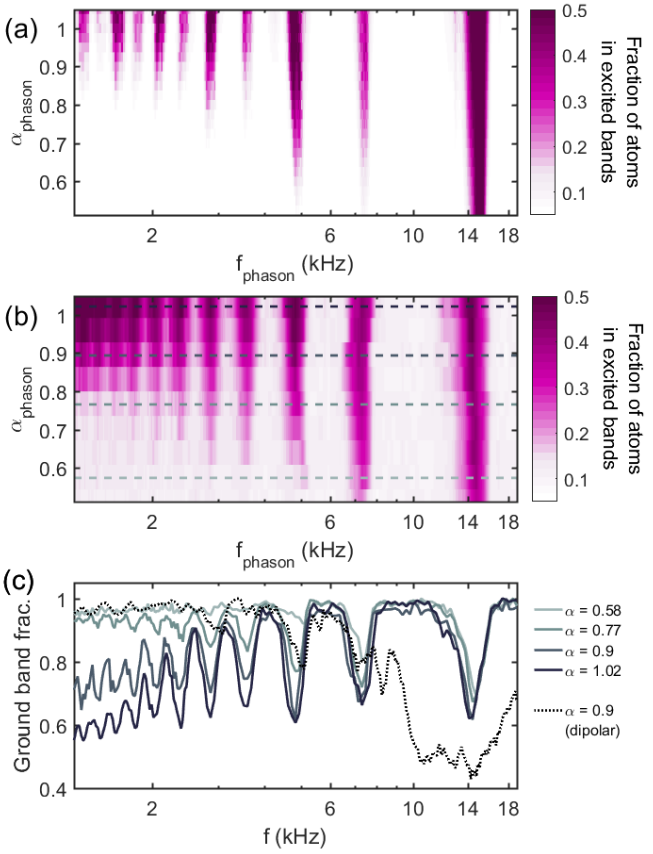

FIG. 3. Amplitude dependence of multiphoton resonances. (a) Theoretical simulation of phasonic spectra for varying drive amplitude α_{phason}. (b) Experimentally measured phasonic spectra for $V_P = 20E_{R,P}$ and varying α_{phason}. Both experiment and theory show the onset of a non-perturbative regime near $\alpha_{\mathrm{th}} = 0.9$. (c) Line cuts of experimental phasonic (solid) and dipolar (dashed) spectra at various α values. Note the extreme power broadening in the dipolar spectrum.

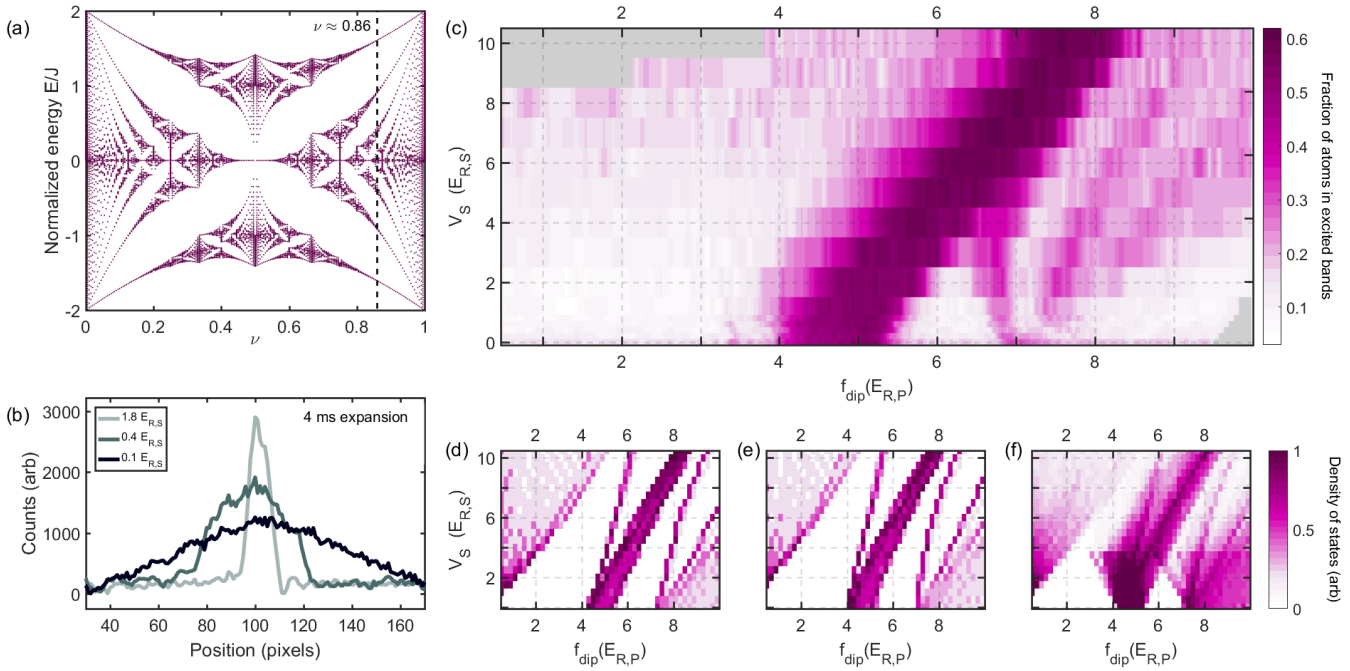

FIG. 4. Spectroscopy of an interacting quasicrystal. (a) Calculated energy spectrum vs. $\nu = \lambda_S/\lambda_P$. Dashed line shows the slice corresponding to the quasicrystal used in this experiment. (b) Post-expansion atomic density distribution at varying disorder strengths V_S, showing the effects of crossing the localization transition. (c) Experimentally measured dipolar excitation spectra for varying V_S/V_P at $\alpha_{\rm dip} = 0.022$, showing spectral minigaps. No data were taken for the gray areas in the upper-left and lower-right. (d) Calculated density of final states for a non-interacting system, starting from a BEC. (e) Calculated density of final states for an interacting BEC; a shift of the resonance line to lower frequencies from Fig. 4(d) is observed. (f) Calculated non-interacting transition density assuming all single-particle orbitals below 1.5 $E_{R,S}$ are initially populated.

The spectroscopic probes of tunable cold-atom quasicrystals which we demonstrate can be deployed to study the rich variety of phenomena arising from quasiperiodicity and interactions. As a consequence of a mapping to the Harper model [29], the non-interacting energy spectrum of a 1D quasicrystal constitutes a slice through the multifractal spectrum of two-dimensional electron gases in the integer quantum Hall regime known as the Hofstadter butterfly [42], plotted in Fig. 4(a). Mapping this fascinating spectrum in an entirely different physical context than high-field 2D Fermi gases, and probing the interplay of interactions and quasiperiodicity are two natural applications for the spectroscopic techniques we describe.

With these goals in mind, we measured the evolution of the spectral response as the strength of quasiperiodicity was increased from zero by tuning V_S/V_P. While the flattened selection rules of phasonic driving are potentially appealing for such a measurement, phasonic driving is not available at $V_S/V_P = 0$ and in any case the strong high-harmonic response complicates the interpretation of phasonic spectra. Therefore for this measurement we chose to use dipolar driving. Tuning of quasiperiodicity was achieved for a fixed V_P by varying the relative strength of the weaker lattice V_S/V_P between zero and one. We note that this range spans a localization transition of the generalized Aubry-André type [17, 28] which has strong effects on transport: Fig. 4(b) shows atomic density distributions after 4 ms of expansion at various values of V_S/V_P, clearly indicating the effects of localization. Fig. 4(c) shows results of dipolar modulation spectroscopy on a 10 $E_{R,P}$ primary lattice at fixed $\alpha_{\rm dip} = 0.022$ and variable V_S, allowing direct measurement of the spectral effects of bichromaticity. We observe the formation of the "minigaps" which are hallmarks of the Hofstadter spectrum.

Comparison of the experimental data (Fig. 4(c)) to the theoretically computed density of states for the non-interacting quasiperiodic lattice (Fig. 4(d)) reveals a number of interesting features. For small V_S, we can clearly identify the three lowermost bands in Fig. 4(d). While the ground band is not reflected in the experimental data, since intraband excitations were not measured, the observed main resonance clearly corresponds to excitations to the first excited band. However, the blueshift (bending to the right) of this resonance with increasing V_S is clearly lower in the experimental data than in the theory of Fig. 4(d). We attribute this effect to interactions; taking them into account on a mean-field level [38], we obtain a reduced blueshift in agreement

with experiment (Fig. 4(e)). Excitations to the second excited band are suppressed by weak coupling matrix elements, since for $V_S = 0$ the dipolar drive couples on-site Wannier states of opposite parity. Nevertheless, the experiment shows a few narrow resonance lines, induced by switching on a finite V_S; we interpret these as a signature of the emergence of minibands. The experimental plot also features an additional resonance line, which merges with the main resonance near $V_S/E_{R,S} = 4$. This feature can be reproduced by a theory which includes the initial presence of excitations as a result of localization-induced non-adiabatic loading (Fig. 4(f)) [38]. This line is effectively a copy of the resonance immediately to its right, corresponding to transitions into these states from the now populated upper edge of the ground band where the density of states shows a pronounced peak (Fig. 4(d)). The observation of the emergence of minigaps in a slice of the Hofstadter butterfly spectrum and the identification of spectral shifts due to interactions in a quasicrystal together constitute the second main result of this report.

The techniques and results we present open up several exciting directions for future work. Most broadly, they enable exploration of numerous open questions concerning quantum quasicrystals. Continuous tuning of the period ratio of the bichromatic lattice would allow direct mapping of the 2D Hofstadter butterfly spectrum. Spectroscopy across the Aubry-André transition may allow study of the effects of localization on heating processes, including in regions with band-dependent localization and single-particle mobility edges [30–33]. Monotonic increase of a phasonic degree of freedom should allow the realization of various topological pumps: a recent proposal suggests high-temperature topological quantized phasonic Thouless pumping of bulk states [43], and the Hofstadter spectrum supports edge states which can be topologically pumped from one end of the system to the other in a single phasonic cycle [22, 44].

In conclusion, we have demonstrated phasonic spectroscopy of a tunable quantum quasicrystal, showed theoretically and experimentally that phasonic excitation efficiently drives non-perturbative high-order multiphoton processes and gives rise to a broad low-frequency absorption feature, mapped the spectral features of a transition from a crystal with extended states to a quasicrystal with localized states, measured the emergence of minigaps in a slice of the Hofstadter spectrum, and identified spectral shifts due to the presence of interactions in a quasicrystal.

The authors thank Zach Geiger, Cora Fujiwara, Kevin Singh, and Max Prichard for experimental assistance and G. Žlabys and U. Schneider for useful discussions. DW acknowledges support from the National Science Foundation (CAREER 1555313), the Office of Naval Research (N00014-16-1-2225), the Army Research Office (PECASE W911NF1410154 and MURI W911NF1710323), and the University of California's Multicampus Research Programs and Initiatives (MRP-19-601445). The work of MR and EA was supported by the European Social Fund under Grant No. 09.3.3-LMT-K-712-01-0051. AE acknowledges funding by the Deutsche Forschungsgemeinschaft (DFG) via the Research Unit FOR 2414 under Project No. 277974659.

[1] D. Shechtman, I. Blech, D. Gratias, and J. W. Cahn, Phys. Rev. Lett. **53**, 1951 (1984).
[2] M. de Boissieu, Chem. Soc. Rev. **41**, 6778 (2012).
[3] P. Bak, Phys. Rev. B **32**, 5764 (1985).
[4] J. E. S. Socolar, T. C. Lubensky, and P. J. Steinhardt, Phys. Rev. B **34**, 3345 (1986).
[5] A. I. Goldman and M. Widom, Annual Review of Physical Chemistry **42**, 685 (1991).
[6] G. G. Naumis and F. Lopez-Rodriguez, Physica B: Condensed Matter **403**, 1755 (2008).
[7] P. A. Thiel and J. M. Dubois, Nature **406**, 570 (2000).
[8] P. Moras, W. Theis, L. Ferrari, S. Gardonio, J. Fujii, K. Horn, and C. Carbone, Phys. Rev. Lett. **96**, 156401 (2006).
[9] Y. E. Kraus and O. Zilberberg, Phys. Rev. Lett. **109**, 116404 (2012).
[10] Y. E. Kraus, Y. Lahini, Z. Ringel, M. Verbin, and O. Zilberberg, Phys. Rev. Lett. **109**, 106402 (2012).
[11] F. Mei, S.-L. Zhu, Z.-M. Zhang, C. H. Oh, and N. Goldman, Phys. Rev. A **85**, 013638 (2012).
[12] M. Verbin, O. Zilberberg, Y. E. Kraus, Y. Lahini, and Y. Silberberg, Phys. Rev. Lett. **110**, 076403 (2013).
[13] K. A. Madsen, E. J. Bergholtz, and P. W. Brouwer, Phys. Rev. B **88**, 125118 (2013).
[14] A. I. Goldman, T. Kong, A. Kreyssig, A. Jesche, M. Ramazanoglu, K. W. Dennis, S. L. Bud'ko, and P. C. Canfield, Nature Materials **12**, 714 (2013).
[15] L.-J. Lang, X. Cai, and S. Chen, Phys. Rev. Lett. **108**, 220401 (2012).
[16] J. E. Lye, L. Fallani, C. Fort, V. Guarrera, M. Modugno, D. S. Wiersma, and M. Inguscio, Phys. Rev. A **75**, 061603 (2007).
[17] G. Roati, C. D'Errico, L. Fallani, M. Fattori, C. Fort, M. Zaccanti, G. Modugno, M. Modugno, and M. Inguscio, Nature **453**, 895 (2008).
[18] M. Schreiber, S. S. Hodgman, P. Bordia, H. P. Lüschen, M. H. Fischer, R. Vosk, E. Altman, U. Schneider, and I. Bloch, arXiv:1501.05661 (2015).
[19] L. Guidoni, C. Triché, P. Verkerk, and G. Grynberg, Phys. Rev. Lett. **79**, 3363 (1997).
[20] L. Guidoni, B. Dépret, A. di Stefano, and P. Verkerk, Phys. Rev. A **60**, R4233 (1999).
[21] T. A. Corcovilos and J. Mittal, Appl. Opt. **58**, 2256 (2019).
[22] K. Singh, K. Saha, S. A. Parameswaran, and D. M. Weld, Phys. Rev. A **92**, 063426 (2015).
[23] B. Gadway, J. Reeves, L. Krinner, and D. Schneble, Phys. Rev. Lett. **110**, 190401 (2013).
[24] K. Viebahn, M. Sbroscia, E. Carter, J.-C. Yu, and U. Schneider, Phys. Rev. Lett. **122**, 110404 (2019).
[25] D. Johnstone, P. Ohberg, and C. W. Duncan, arXiv:1904.12870 (2019).
[26] J. A. Kromer, M. Schmiedeberg, J. Roth, and H. Stark, Phys. Rev. Lett. **108**, 218301 (2012).

[27] M. Widom, Philosophical Magazine **88**, 2339 (2008).
[28] S. Aubry and G. André, Ann. Isr. Phys. Soc. **3**, 133 (1980).
[29] P. G. Harper, Proceedings of the Physical Society. Section A **68**, 874 (1955).
[30] D. J. Boers, B. Goedeke, D. Hinrichs, and M. Holthaus, Phys. Rev. A **75**, 063404 (2007).
[31] X. Li, X. Li, and S. Das Sarma, Phys. Rev. B **96**, 085119 (2017).
[32] H. P. Lüschen, S. Scherg, T. Kohlert, M. Schreiber, P. Bordia, X. Li, S. Das Sarma, and I. Bloch, Phys. Rev. Lett. **120**, 160404 (2018).
[33] T. Kohlert, S. Scherg, X. Li, H. P. Lüschen, S. Das Sarma, I. Bloch, and M. Aidelsburger, Phys. Rev. Lett. **122**, 170403 (2019).
[34] A. Eckardt, Rev. Mod. Phys. **89**, 011004 (2017).
[35] M. Weinberg, C. Ölschläger, C. Sträter, S. Prelle, A. Eckardt, K. Sengstock, and J. Simonet, Phys. Rev. A **92**, 043621 (2015).
[36] M. Reitter, J. Näger, K. Wintersperger, C. Sträter, I. Bloch, A. Eckardt, and U. Schneider, Phys. Rev. Lett. **119**, 200402 (2017).
[37] D. McKay, M. White, and B. DeMarco, Phys. Rev. A **79**, 063605 (2009).
[38] See Supplemental Material for a discussion on numerical calculations and an analytic explanation for high-order phasonic multiphoton resonances.
[39] C. Sträter and A. Eckardt, Z. Naturforsch. A **71**, 909 (2016).
[40] I. Limas, G. Naumis, F. Salazar, and C. Wang, Physics Letters A **337**, 141 (2005).
[41] S.-n. Zhu, Y.-y. Zhu, and N.-b. Ming, Science **278**, 843 (1997).
[42] D. R. Hofstadter, Phys. Rev. B **14**, 2239 (1976).
[43] N. H. Lindner, E. Berg, and M. S. Rudner, Phys. Rev. X **7**, 011018 (2017).
[44] Y. E. Kraus, Y. Lahini, Z. Ringel, M. Verbin, and O. Zilberberg, Phys. Rev. Lett. **109**, 106402 (2012).